scientific reports

Check for updates

OPEN

# Screening of electrospun PS/PCL scaffolds for three-dimensional triple negative breast cancer cell culture: impact of solvent, hydrophobicity, and setup orientation

Sira Ausellé-Bosch[1], Marta Pardo[1], Marta Pareja[1], Emma Polonio-Alcalá[2] & Teresa Puig[1]✉

**Triple-Negative Breast Cancer (TNBC) presents a significant challenge due to its aggressiveness and lack of targeted therapies. Understanding the interaction between TNBC cells and the extracellular matrix (ECM) in three-dimensional (3D) culture systems is vital for developing accurate *in vitro* models. This study explores the impact of electrospinning setup orientation, solvent selection, and polymer composition on scaffold design and TNBC cell culture. Various polystyrene (PS) and poly-ε-caprolactone (PCL) combinations were electrospun using different solvent combinations (dichloromethane/dimethylformamide (DCM/DMF), tetrahydrofuran/dimethylformamide (THF/DMF), chloroform/dichloromethane (Chl/DCM) and acetone) and setup orientations (vertical, horizontal). Scaffolds were characterized using Scanning Electron Microscopy (SEM) to assess fiber diameter and pore size. Cell proliferation and morphology were analyzed through MTT assay, SEM and Confocal Laser Scanning Microscopy (CLSM). Pore area and fiber diameter were influenced by solvent combination (THF/DMF < DCM/DMF < acetone < Chl/DCM) and orientation setup (horizontal < vertical). Sterilization assay revealed that 1-hour immersion in 70% ethanol followed by 30 min ultra-violet (UV) light exposure achieved sterilization with minimal scaffold degradation. High proliferation with no significant reduction compared to monolayer culture was found in some scaffolds and variability in cell morphology between scaffolds was also detected. Results highlight the critical role of scaffold printing parameters for 3D TNBC cell culture. Electrospun PS/PCL 40/60 scaffolds dissolved in DCM/DMF are promising *in vitro* models, providing a valuable tool for cancer research.**

**Keywords** Electrospinning, Polystyrene, Poly-ε-caprolactone, Scaffolds, Three-dimensional cell culture, Fiber morphology

Breast cancer (BC) is the most frequently diagnosed malignancy and the leading cause of cancer-related mortality among women worldwide[1]. Triple-negative breast cancer (TNBC) accounts for 15–20% of BC cases, predominantly affecting younger women and associated with a poorer prognosis and higher relapse rates[2]. Characterized by an immunohistochemical profile lacking the overexpression of estrogen and progesterone receptors, and human epidermal growth factor 2 receptor (HER2), TNBC is unresponsive to the targeted therapies typically employed in other BC subtypes. Therefore, this subtype presents a significant clinical challenge due to its aggressive nature and the absence of targeted therapy, requiring a multimodal approach that includes chemotherapy, surgery, and radiotherapy as the standard of care[2]. Despite initial response rates, a substantial proportion of patients experience disease recurrence, underscoring the urgent need for the identification of novel biomarkers and the development of new therapeutic strategies[3]. Cancer stem cell (CSCs) subpopulation, due to its tumorigenic properties, self-renewal ability and differentiation into non-stem cancer cells, has been

[1]New Therapeutic Targets Laboratory (TargetsLab) – Oncology Unit, Medical Sciences Department, University of Girona, Girona, Spain. [2]Precision Oncology Group (OncoGIR-Pro), Girona Biomedical Research Institute (IDIBGI-CERCA), Girona, Spain. ✉email: teresa.puig@udg.edu

linked to tumor development, metastasis and drug resistance[4]. Thus, CSCs could be a potential target for future treatments, and, developing supports that enhance their growth is essential to study them.

*In vitro* cancer studies are traditionally conducted using two-dimensional (2D) cell culture systems due to their cost- and time-efficiency[5,6]. However, advancements in three-dimensional (3D) cell culture technologies have been developed to enhance the accuracy and relevance of these studies. 3D techniques replicate the complex structural architecture of the extracellular matrix (ECM) more effectively, providing a closer approximation of the *in vivo* tumor microenvironment compared to 2D cultures[5–8]. This improved mimicry results in more accurate representations of *in vivo* characteristics such as cell proliferation rate, cell morphology, gene expression, and CSCs growth in different cancer types[9–11].

A widely employed method for developing 3D cell culture models involves the use of scaffolds —solid supports fabricated from natural or synthetic materials— which can be produced via electrospinning techniques. Electrospun scaffolds offer a structural framework with fiber sizes comparable to the ECM that, along with high porosity and surface area, enhance cell attachment and growth[12]. Synthetic polymers such as polystyrene (PS) and poly-ε-caprolactone (PCL) are commonly used in electrospinning due to their favorable properties such as viscoelastic properties, melting points and biocompatibility, which make them suitable candidates for cell culture and biomedical studies[13–15]. PCL is a well-established, biocompatible polymer employed for the fabrication of electrospun scaffolds, due to its great malleability and viscoelastic properties[7,16]. PS is used in electrospinning for its affordability, versatility and intrinsic characteristics[17]. Hence, the combination of PS/PCL could provide scaffolds with enhanced mechanical properties which supports 3D cell culture. These polymers can be processed using various solvents, including dichloromethane (DCM), dimethylformamide (DMF), chloroform (Chl), acetone, and tetrahydrofuran (THF). Numerous studies have reported that the choice of solvent for electrospinning can significantly influence the fiber diameter and pore area of the scaffold, making it a crucial variable in achieving the desired scaffold characteristics[14,15,18–20]. Additionally, the orientation of the electrospinning setup, whether vertical or horizontal, can lead to differences in the final spun scaffolds[21]. However, despite extensive research on electrospun scaffolds, few studies have systematically analyzed the critical role of polymer composition, solvent selection, and electrospinning setup orientation in scaffold fabrication and how these parameters collectively influence scaffold architecture and cell behavior. Understanding these combined effects is key to enhancing scaffold performance for 3D cell culture applications.

Therefore, this study aims to assess the impact of polymer composition, solvent combinations and setup orientation on the feasibility of 3D TNBC cell culture. To this end, sixteen polymer solutions with varying PS and PCL concentrations were manufactured using different solvent combinations (DCM/DMF (1:3), THF/DMF (1:3), Chl/DCM (7:3) and acetone) and electrospun in both vertical and horizontal setup orientations. The resulting scaffolds were characterized and seeded with a TNBC cell line to evaluate the suitability of electrospun PS/PCL scaffolds as a novel tool for 3D BC cell culture.

## Materials and methods

### Chemical and reagents

Polycaprolactone (PCL, Mn 80,000 g/mol, #440744), polystyrene (PS, Mw 192,000 g/mol, #430102), dichloromethane (DCM, >99% (GC), #24233), 3-(4,5-dimethyl-2-thiazolyl)-2,5-diphenyl-2 H-tetrazolium bromide (MTT; #M2128), paraformaldehyde (PFA; #441244), glutaraldehyde, sodium cacodylate and Triton™ X-100 (#93443) were purchased from Sigma-Aldrich (St. Louis, MO, USA). N-N dimethylformamide (DMF; 99.9% GLR, #DMFO-P0P), ethanol absolute (AGR; #ETHA-9TA), chloroform (Chl; AGR; #CHLF-S0A) and tetrahydrofuran (HPLC GGR; #TETR-0GH) were obtained from Labkem, Labbox Labware S.L. (Barcelona, Spain). BSA Fraction V pH for Western blotting (#6588) and Acetone (ACS; #131007.1211) were procured from PanReac AppliChem (Gatersleben, Germany). Dulbecco's Modification of Eagle's Medium (DMEM; #10-013-CV) and phosphate-buffered saline (PBS; #21-031-CV) were obtained from Corning (New York, USA). Fetal bovine serum (FBS; #SH30066.03) and penicillin/streptomycin (10.000 U/mL/10.000 µg/mL; #SV30010) were purchased from HyClone (Logan, UT, USA). Trypsin (10×; #X0930-100) was obtained from Dutscher (Bernolsheim, France). Rhodamine-phalloidin was purchased from Cytoskeleton Inc. (Denver, CO, USA), and 4,6-diamidino-2-phenylindole (DAPI) was obtained from BD Pharmingen (Franklin Lakes, NJ, USA).

### Cell line

MDA-MB-231 human TNBC cell line, a mesenchymal stem-like subtype, was purchased from the American Type Culture Collection (ATCC, Rockville, MD, USA). Cells were cultured in DMEM medium supplemented with 10% FBS and 50 U/mL penicillin/streptomycin. Cell environment was kept at 37 °C with 5% CO2. Continuous monitoring and systematic checks for mycoplasma contamination were performed to maintain the integrity of the cell line.

### Manufacturing of electrospun fibers

Various mixtures of PS and PCL (Table S1) were dissolved in solvent A (DCM/DFM (1:3)), solvent B (TFH/DMF (1:3)), solvent C (Chl/DCM (7:3)) and solvent D (acetone) at a concentration of 15% (w/v) for 24 h at 50 °C with continuous stirring. For vertical set orientation, the solutions were placed in a 5 mL syringe, connected via a polytetrafluoroethylene tube (1 mm inner diameter) to a stainless steel 22G (0.41 mm inner diameter) or 18G needle (0.84 mm inner diameter) and electrospun using the equipment from Spraybase (Dublin, Ireland) managed using Syringe Pump Pro software (New Era Pump Systems, Farmingdale, NY, USA). For horizontal setup orientation, solutions were placed in a 5 mL syringe directly attached to a stainless steel 22G (0.41 mm inner diameter) or 18G needle (0.84 mm inner diameter) and electrospun using a device from Linari Engineering (Pisa, Italy). Electrospinning parameters were selected to consistently form the Taylor cone during electrospinning (Table S1). Additionally, environmental conditions such as temperature (23 °C to 27 °C) and

humidity (20 to 60%) were controlled. The resulting structures were left at room temperature for at least 24 h to ensure proper solvent evaporation and cut into squares of 2.56 $cm^2$.

### Scaffolds microarchitecture observation

Non-sterilized scaffolds were cut and coated with gold using a K950 turbo evaporator (Emitech, Kent, UK). The structures were dried with a K850 CPD critical point dryer (Emitech) and coated with gold using the K950 turbo evaporator (Emitech). Observations were conducted using an S4100 field emission scanning electron microscope (SEM; Hitachi, Tokyo, Japan) capturing the images with Quartz PCI software (Quartz, Vancouver, Canada) or using a Tescan Clara SEM (Tescan Group, Brno, Czech Republic). MATLAB software (MathWorks; Natick, MA, USA) was used to determine fiber diameter, and pore area. Briefly, filament diameter was measured by calculating the perpendicular distance between the top and bottom of the filament of eight random fibers from each image, without including beads in the measurements. Pore area was calculated by manually tracing the pore shapes on three randomly selected pores from each image.

### Sterilization and degradation assay

Scaffolds were weighed using a Sartorius ED224S analytical balance (Sartorius, Göttingen, Germany). Then, they were sterilized using different combinations of ultra-violet (UV) light exposure and immersion to a 70% (v/v) ethanol absolute solution diluted in distilled water (Table S2). Upon sterilization, scaffolds were rinsed twice with PBS and placed in non-adherent 12-well plates (Sartstedt, Nümbrecht, Germany). Subsequently, 2mL of supplemented medium without antibiotics was added to each well and incubated for 7 days to check for contaminants. Following incubation, the scaffolds were washed twice with PBS, air-dried and reweighted. Non-sterilized scaffolds served as positive control and media without control as negative control. Sterilization was confirmed by no change in medium color and no presence of clouding after 7 days of incubation.

### Cell proliferation assay

Scaffolds were sterilized by immersing them in 70% ethanol for 1 h, followed by two washes with PBS and exposure to UV light for 30 min on each side. Subsequently, the scaffolds were placed into non-adherent 12-well plates (Sartstedt) and soaked in supplemented medium overnight (ON). Following this, 1200 MDA–MB–231 cells were seeded onto the scaffolds for 3D culture using the drop-by-drop method, as previously described[22]or into adherent 12-well plates (Sartstedt) for monolayer culture. Cells were maintained for 18 days replacing medium every six days. Samples were collected every three days and a MTT assay was conducted to assess cell viability, as previously reported[9]. Briefly, the adherent wells and scaffolds were washed twice with PBS, and the scaffolds were placed to new wells to ensure only attached cells would be tested. Then, 1 mL of DMEM and 100 µL of MTT (Sigma-Aldrich, St. Louis, MO, USA) were added, and the samples were incubated for 150 min at 37ºC and 5% CO2 atmosphere where viable cells converted MTT into formazan crystals. After incubation, the formazan crystals were dissolved using 1 mL of DMSO (Sigma-Aldrich, St. Louis, MO, USA) with shaking. Three 100 µL aliquots from each well were then transferred to a 96-well plate and absorbance was measured at 570 nm using the Benchmark Plus microplate spectrophotometer (Bio-Rad, Hercules, CA, USA).

### Three-dimensional cell culture and morphology assessment

Sterilized scaffolds were placed in non-adherent 12-well plates and soaked in medium ON to promote cell attachment. The pertinent cell density (2000 cells/scaffold) was prepared in 50 µL of medium and cells were seeded on scaffolds as described[22]. Cells were maintained for 15 days, replacing the medium every five days, and cell attachment to fibers and cell proliferation was evaluated through CLSM and SEM imaging.

For CLSM observation, samples were fixed with a 4% paraformaldehyde solution (w/v), permeabilized using 0.2% Triton™ X-100 (v/v), blocked with a 3% BSA solution (w/v), and stained with rhodamine-phalloidin (1:250) and DAPI (1:1000). Fluorescence imaging was performed using an A1R confocal laser scanning microscope (CLSM; Nikon, Tokyo, Japan), and images were captured with Nikon NIS-Elements AR v4.10 software (Nikon). The circularity of the nucleus and cytoplasm was analyzed using MATLAB software (MathWorks; Natick, MA, USA). Three replicates of each scaffold were imaged and five cells were randomly selected for perimeter and area measurements. Circularity was determined using a formula designed to give a value of 1 to a perfect circle and values close to 0 for elongated nucleus or cytoplasm[18].

$$Circularity = \frac{4 \cdot \pi \cdot area}{perimeter^2}$$

For SEM imaging, the seeded samples were fixed with a 2.5% (v/v) glutaraldehyde solution in 0.1 M sodium cacodylate (pH 7.4), rinsed with 0.1 M sodium cacodylate, and dehydrated through a series of ethanol concentrations (50%, 75%, 80%, 90%, 95%, and 100%). The structures were then dried with a K850 CPD critical point dryer (Emitech) and coated with gold using the K950 turbo evaporator (Emitech). Observations were conducted using an S4100 field emission scanning electron microscope (SEM; Hitachi, Tokyo, Japan) capturing the images with Quartz PCI software (Quartz, Vancouver, Canada) or using a Tescan Clara SEM (Tescan Group, Brno, Czech Republic).

### Water contact angle (WCA) measurement

Electrospun PS/PCL scaffolds were cut into 150 $mm^2$ sections and positioned in a setup designed for Water Contact Angle (WAC) measurement. As previously reported[23]a 3 µL droplet of Milli-Q deionized water was carefully deposited onto each scaffold using a micropipette. After the droplet stabilized, a side-view image was

captured and analyzed using ImageJ software. The contact angles (CAs) on both the left and right sides of three separate droplets were measured to ensure measurement consistency, and their average value was calculated.

### Dynamic mechanic analysis (DMA)

Scaffolds were cut into 15 × 5 mm and placed into a Mettler Toledo DMA/SDTA 861 equipped with dual cantilever tools (Mettler-Toledo; Columbus, OH, USA). The test was conducted at ambient temperature (22°C) with a frequency of 1 Hz. An amplitude sweep was applied, incrementally increasing the displacement up to 100 µm at tensile mode. The Storage modulus (E') was evaluated for a displacement amplitude of 1 µm, corresponding to a strain of 0.018%, within the viscoelastic region.

### Statistical analysis

Statistical analysis was conducted using GraphPad Prism software (Version 10.2.1; GraphPad Software, La Jolla, CA, USA). Experiments were repeated at least three times, and data were expressed as the mean ± standard error of the mean (SEM). Normality of data was studied using Shapiro-Wilk test and distribution of SD was tested by Brown-Forsythe test. For two-group comparisons, parametric data were evaluated using the Student's t-test, while non-parametric data were assessed with the Mann-Whitney U test. For comparisons involving more than two groups, parametric data were analyzed using one-way analysis of variance (ANOVA) with Tamhane's T2 or Šídák post hoc tests, and non-parametric data were evaluated using the Kruskal-Wallis test. Significance levels were defined as $p < 0.050$ and were indicated as follows: $p < 0.050$ (*), $p < 0.010$ (**), and $p < 0.001$ (***).

## Results

### Electrospun PS/PCL scaffolds characterization

To study the microstructure of the spun scaffolds, all meshes were imaged by Scanning Electronic Microscopy (SEM) (Fig. 1). Scaffolds were visualized from both bottom and top sides, to ensure uniformity across sides (data not shown). Notably, certain scaffolds exhibited the presence of spherical non-filamentous polymer formations, referred to as beads (Fig. 1a, g-l and o).

Results revealed significant variations in pore area and fiber diameter based on the solvent combination and the orientation of the electrospinning setup (vertical vs. horizontal) (Table 1). A consistent trend was observed, where scaffolds produced in the vertical orientation (191.90 ± 72.36 µm) exhibited larger pore areas compared to those spun in the horizontal orientation (151.40 ± 55.59 $\mu m^2$) (Figure S1a). This trend was also reflected in the fiber diameter (Figure S1d), where vertical orientation resulted in larger fibers (1.71 ± 0.31 µm) compared to the horizontal orientation (1.27 ± 0.26 µm).

In terms of solvent combinations, scaffolds produced using solvent C and D exhibited significantly larger pore areas and fiber diameters compared to those fabricated with solvents A and B (Figure S1b, S1e). Specifically, solvent C and D-based scaffolds had a higher average pore area and fiber diameter than scaffolds produced with the other solvents, being in solvent C statistically significant.

When examining the impact of polymer composition (PS/PCL), an increasing trend in fiber diameter was observed with lower PS and higher PCL concentrations (Figure S1f). The average fiber diameter ranged from 1.96 ± 0.70 µm to 0.82 ± 0.08 µm. However, no clear relationship between polymer composition and pore area was observed (Figure S1c).

Overall, these findings indicate that both the solvent combination and the orientation of the electrospinning setup have a significant impact on the structural characteristics of the scaffolds. These factors play a crucial role in determining the suitability of electrospun scaffolds for 3D TNBC cell culture, with the potential to influence cell attachment, growth, and overall culture outcomes.

For the following experimental, bead-free scaffolds were selected. These bead structures are characterized by a lower surface area-to-volume ratio compared to the typical fibrous scaffold, thereby providing a less favorable substrate for cell attachment[24].

### Sterilization method on PS/PCL scaffolds for cell culture

To determine the optimal sterilization method for bead-free scaffolds, we conducted a sterilization assay aimed at achieving effective sterilization to prepare them for cell culture with minimal impact on scaffold degradation. Among the tested combinations of UV light exposure and 70% ethanol immersion (Table S2), consistent sterilization was achieved across all scaffolds with either 1–4 h of 70% ethanol immersion followed by 30 min of UV exposure on each side, as well as with 16 h of 70% ethanol immersion, regardless of subsequent UV exposure (Table S3).

Additionally, a weight degradation test was carried out to determine potential alterations in PS/PCL scaffolds produced by sterilization. Overall, the results indicated a 2–6% increase in scaffold weight, with significantly greater weight increase observed in more aggressive sterilization methods (16-hour immersion in 70% ethanol followed by 30 min of UV exposure) compared to less aggressive ones (UV exposure alone, 1-hour immersion in 70% ethanol, and the combined condition) (Fig. 2). Further analysis of individual scaffolds (Figure S2) revealed a notably higher weight increase in solvent A-based scaffolds compared to solvent C and D-based scaffolds (Figure S3a). Additionally, increased PS and decreased PCL concentration correlated with significantly greater weight increases (Figure S3b). Finally, no significant differences were seen when concerning setup orientation (Figure S3c). Therefore, a clear impact of solvent combination and polymer composition on scaffold weight degradation is determined.

Taking the results into account, the sterilization method consisting in 1 h immersion in 70% ethanol followed by 30 min exposure to UV light on each side was selected for subsequent analysis. To assess if microstructural changes were induced by sterilization method scaffolds were characterized through SEM microscopy and fiber diameter and pore area were analyzed (Fig. 3a-h). Visually, the SEM analysis revealed a clear microstructural

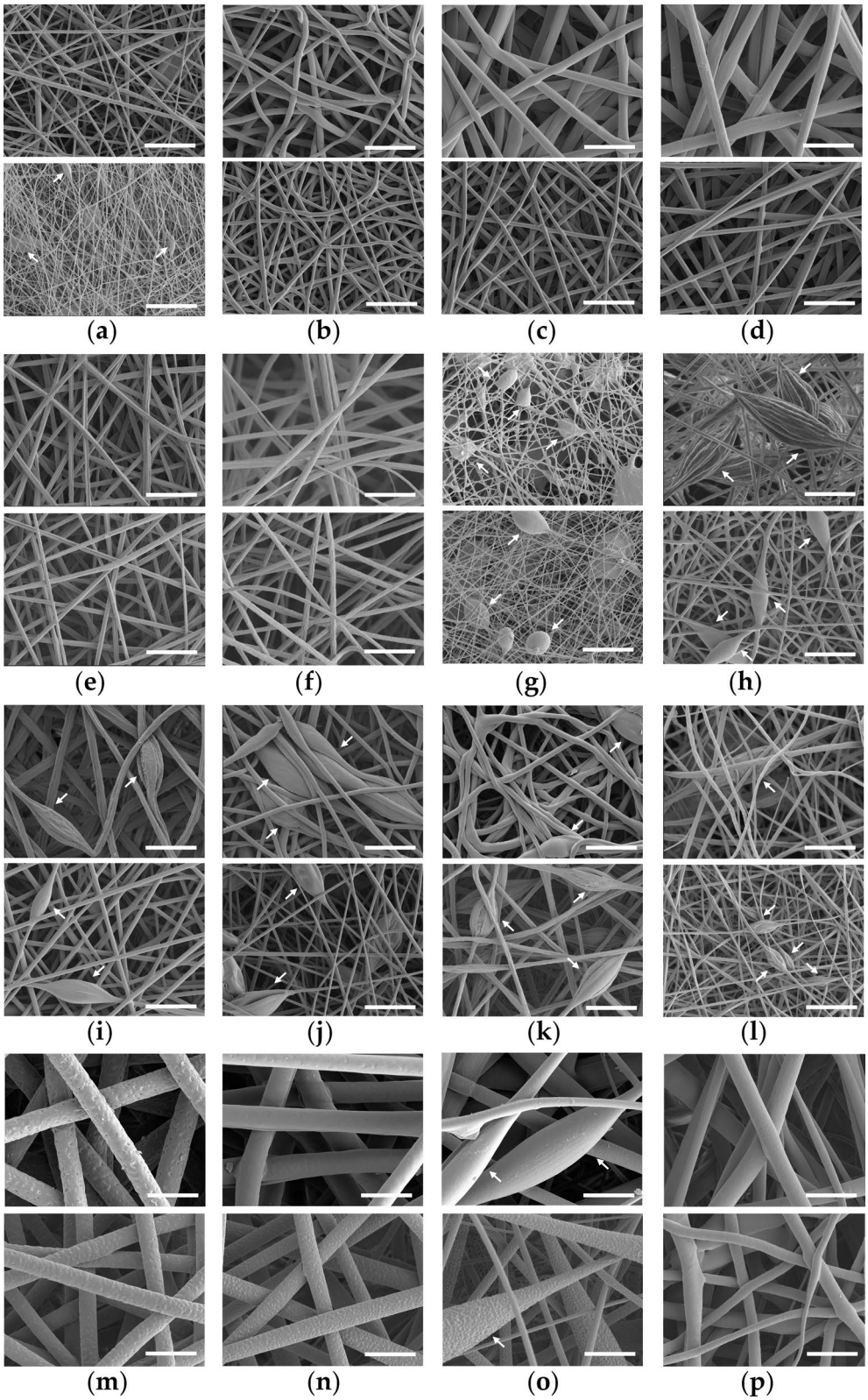


**Fig. 1**. Scanning electronic microscopy (SEM) images from (**a**) A1 scaffolds (**b**) A2 scaffolds, (**c**) A3 scaffolds, (**d**) A4 scaffolds, (**e**) A5 scaffolds, (**f**) A6 scaffolds, (**g**) B1 scaffolds, (**h**) B2 scaffolds, (**i**) B3 scaffolds, (**j**) B4 scaffolds, (**k**) B5 scaffolds, (**l**) B6 scaffolds, (**m**) C1 scaffolds, (**n**) C2 scaffolds, (**o**) C3 scaffolds and (**p**) D1 scaffolds spun in vertical (upper panel) and horizontal (lower panel) setup orientation. Beads are indicated by arrows. Scale bar: 10 μm. Images are representative of three independent experiments in triplicate ($n = 3$).

| Composition | Abr. | Vertical set orientation | | Horizontal set orientation | |
|---|---|---|---|---|---|
| | | Pore area (μm²) | Fiber diameter (μm) | Pore area (μm²) | Fiber diameter (μm) |
| PS/PCL 0/100 (DCM/DMF) | A1 | 38.65 ± 7.86 | 0.70 ± 0.03 *# | 11.10 ± 2.37*##$$† *##$$ | 0.24 ± 0.01*##$† *##† |
| PS/PCL 20/80 (DCM/DMF) | A2 | 40.85 ± 6.77 | 1.11 ± 0.09 | 22.61 ± 1.29#$$#$ | 1.01 ± 0.16 |
| PS/PCL 40/60 (DCM/DMF) | A3 | 80.66 ± 7.19 | 1.49 ± 0.24 | 43.40 ± 1.82 | 1.04 ± 0.12 |
| PS/PCL 60/40 (DCM/DMF) | A4 | 80.40 ± 1.81 | 1.80 ± 0.39 | 78.60 ± 8.42 | 1.24 ± 0.04 |
| PS/PCL 80/20 (DCM/DMF) | A5 | 56.77 ± 8.09 | 1.15 ± 0.07 | 52.40 ± 9.13 | 0.97 ± 0.06 |
| PS/PCL 100/0 (DCM/DMF) | A6 | 53.85 ± 11.16 | 0.99 ± 0.21 | 43.76 ± 9.95 | 0.78 ± 0.15 |
| PS/PCL 0/100 (THF/DMF) | B1 | 10.75 ± 0.47*##$$† #$ | 0.33 ± 0.01*#† *# | 9.16 ± 0.53 *#$$† *##$$ | 0.26 ± 0.02*##$† *##† |
| PS/PCL 20/80 (THF/DMF) | B2 | 43.54 ± 5.55 | 0.76 ± 0.03 | 29.06 ± 3.67#$ | 0.65 ± 0.01*# |
| PS/PCL 40/60 (THF/DMF) | B3 | 56.99 ± 9.68 | 1.50 ± 0.04 | 48.75 ± 0.34 | 0.88 ± 0.04 |
| PS/PCL 60/40 (THF/DMF) | B4 | 32.19 ± 0.71$ | 1.06 ± 0.03 | 74.71 ± 4.00 | 0.69 ± 0.02*# |
| PS/PCL 80/20 (THF/DMF) | B5 | 48.96 ± 2.59 | 1.25 ± 0.03 | 78.85 ± 4.69 | 0.89 ± 0.19 |
| PS/PCL 100/0 (THF/DMF) | B6 | 44.18 ± 4.28 | 0.91 ± 0.03 | 26.42 ± 0.47#$ #$ | 0.61 ± 0.01*# *# |
| PS/PCL 0/100 (Chl/DCM) | C1 | 345.35 ± 28.46 | 4.38 ± 0.19 | 290.78 ± 30.44 | 3.54 ± 0.06 |
| PS/PCL 20/80 (Chl/DCM) | C2 | 772.12 ± 15.44 | 4.59 ± 0.13 | 675.27 ± 50.79 | 3.65 ± 0.09 |
| PS/PCL 40/60 (Chl/DCM) | C3 | 971.12 ± 64.94 | 2.45 ± 0.10 | 691.39 ± 34.84 | 1.39 ± 0.02 |
| PS/PCL 0/100 (Acetone) | D1 | 385.05 ± 2.02 | 2.89 ± 0.06 | 246.54 ± 22.51 | 2.53 ± 0.13 |

**Table 1**. Pore area and fiber diameter of scaffolds. Data are presented as mean ± SEM of three independent experiments in triplicate ($n = 3$). Levels of statistically significance are indicated as *($p < 0.050$), **($p < 0.010$), and ***($p < 0.001$). The symbol * indicates the comparison with C1 scaffolds, the symbol # indicates the comparison with C2 scaffolds, the symbol $ indicates the comparison with C3 scaffolds, and the symbol † indicates the comparison with D1 scaffolds, spun in vertical (first) or horizontal (second). Scaffolds were abbreviated (Abr.) with letters representing the solvent used (A-D) and numbers indicating the PS/PCL composition (1–6).

degeneration including fused (Fig. 3b) and broken (Fig. 3c) fibers, and sheet-like connections between them (Fig. 3d).

Quantitively, results showed a general trend of increased fiber diameter and pore area in scaffolds after sterilization, being significantly remarkable in only some of the scaffolds (Table 2).

When comparing pore area and fiber diameter data within scaffolds after the sterilization method, we can still see a trend of higher pore area and fiber diameter in vertically spun scaffolds compared to horizontally spun scaffolds (Figure S4a, S4d). Additionally, scaffolds produced with C and D solvents still exhibited significantly larger pore areas and fiber diameters compared to those fabricated with solvent A (Figure S4b, S4e).

Furthermore, the influence of polymer composition on fiber diameter persisted (Figure S4f), with lower PS and higher PCL concentrations correlating with a trend of increased fiber dimeter (ranging from 3.10 ± 0.39 μm to 1.22 ± 0.11 μm). However, similar to observations before sterilization, no clear relation between polymer composition and pore area was evident (Figure S4c), as demonstrated by the varying average pore areas across different PS/PCL concentrations.

## TNBC cell proliferation on PS/PCL scaffolds

As previously mentioned, different factors can influence the microstructure of electrospun scaffolds, which in turn impacts the cell adhesion and growth of TNBC cells in a 3D environment. To assess which scaffold microenvironment was optimal for cell growth, MDA-MB-231 TNBC cells were seeded on both 2D surfaces and the studied scaffolds and cell viability was studied over an 18-day period.

Results demonstrated no significant differences in cell proliferation ratio between the scaffolds and 2D surfaces during the initial days of culture. However, as cell confluence increased (from day 12), some differences between cell culture supports could be seen (Fig. 4). At day 12, MDA-MB-231 cells cultured on 2D surfaces already showed a higher proliferation compared to A5 ($p = 0.02$) and D1 ($p = 0.04$) scaffolds spun in horizontal. At day 15, cells cultured on 2D presented a higher proliferation compared to all scaffolds (p-value ranging from < 0.001 to 0.04), adopting an exponential cell growth.

Finally, when comparing the proliferation of cells on each scaffold to 2D conditions at 18 days of culture, differences in cell proliferation across the various microstructures were observed. In this regard, only A2, A3 and C2 scaffolds, spun in horizontal and vertical, reached an exponential cell growth slope that did not statistically differ from cells cultured in monolayer conditions, highlighting their potential as optimal environments for TNBC cell culture in further experimentation.

## TNBC cell morphology on PS/PCL scaffolds

Scaffolds serve as a physical support that closely mimics the ECM microenvironment, enabling cells to adhere to the fibers and establish connections between them. To elucidate whether there were morphological differences between the six scaffolds with higher cell proliferation, MDA-MB-231 cells were cultured for 15 days on these matrices and subsequently imaged through Confocal Laser Scanning Microscopy (CLSM) and SEM (Fig. 5).

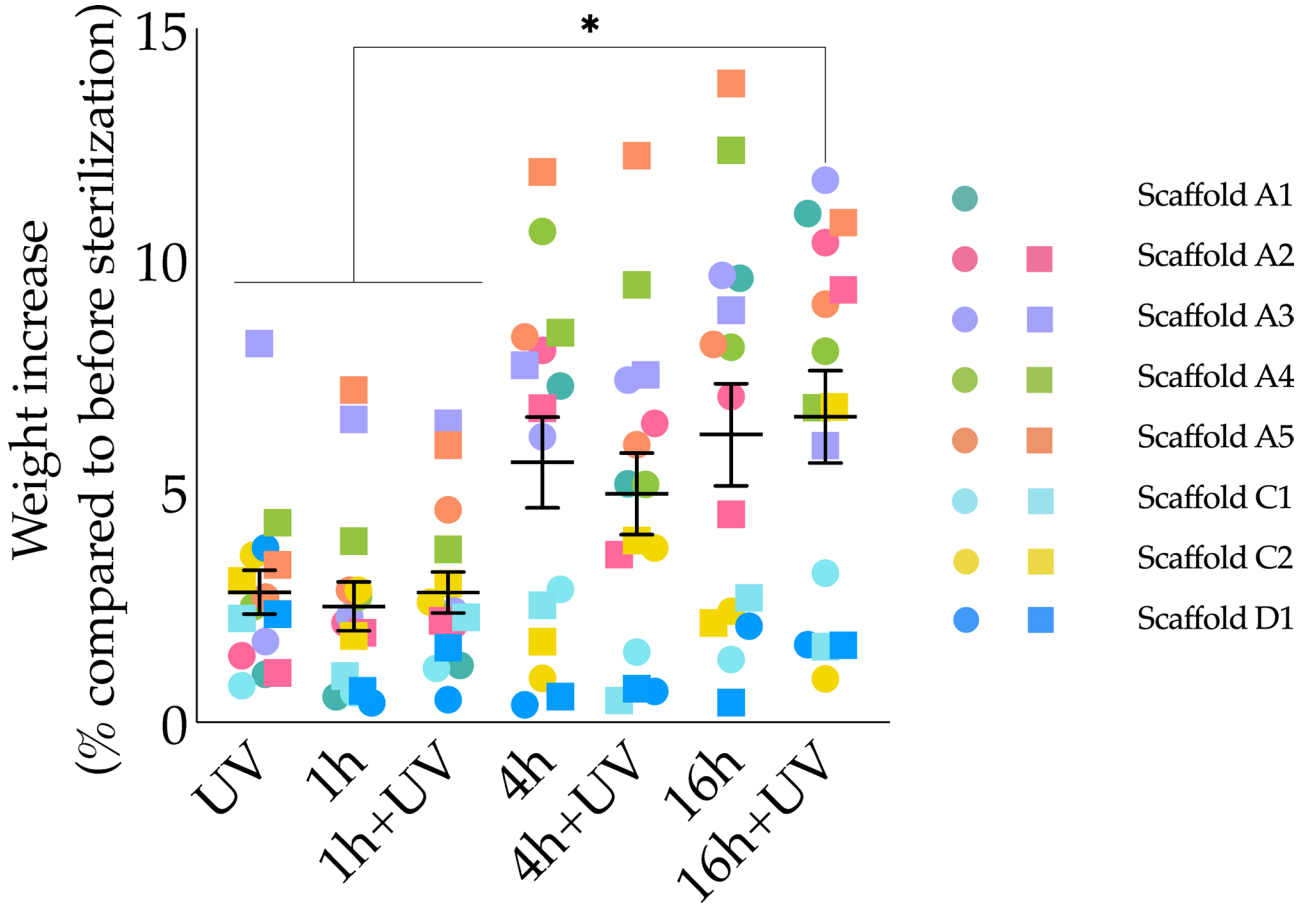


**Fig. 2**. Sterilization effect on PS/PCL scaffolds weight. Data are represented as mean ± SEM of all the scaffolds from three independent experiments in triplicate ($n = 3$). Levels of statistically significance are indicated as *($p < 0.050$), **($p < 0.010$), and ***($p < 0.001$). Setup orientation is represented by symbol shape (circle: vertical; square: horizontal).

Through SEM imaging, we aimed to examine the interaction of TNBC cells between them and the fibers. Results confirmed that cells adhered and wrapped to the manufactured fibers. Additionally, interactions between cells through their connections with the fibers were observed across all the scaffolds studied.

To further assess cytoplasmatic and nuclear morphology, actin cytoplasm and nucleus were stained and imaged through CLSM. The imaging revealed visual differences in cell morphology between cells cultured on different scaffolds (Fig. 5a). On A2 and C2 scaffolds, regardless of the setup orientation, cells exhibited a more rounded shape in both nucleus and cytoplasm, which is consistent with typical morphology observed in monolayer cultures. In contrast, when wells were cultured in A3 scaffolds, cells displayed a more elongated cytoplasm with prolongations, whereas no qualitative differences were observed in nucleus. Notably, in all PS/PCL scaffolds studied, cell culture occurred at different depths within the scaffold, as evidenced by some cells appearing unfocused in the Z-plane of the confocal microscopy.

Quantitative analysis was performed to assess the degree of cytoplasm and nucleus circularity. Consistent with the descriptive microscopic observation, A3 scaffolds presented a significantly lower cytoplasm circularity than A2 and C2 scaffolds (Fig. 5b). However, no notable changes were observed in nucleus morphology across scaffolds (Fig. 5c).

To assess whether scaffold hydrophobicity influences cell morphology, a Water Contact Angle (WCA) measurements were performed (Fig. 6a). Results revealed no significant differences in contact angle among the studied scaffolds, suggesting that polymer concentration, solvent selection, and setup orientation do not substantially impact scaffold hydrophobicity. Additionally, a correlation analysis between WCA and cell morphology showed no significant relationship ($r$ = -0.532, $p = 0.278$), reinforcing the notion that surface hydrophobicity is not determinant for cell shape.

Since mechanical properties play a crucial role in cellular behavior, scaffold stiffness was evaluated to determine its potential effect on cell morphology. Dynamic mechanic analysis (DMA) revealed Storage modulus (E') remained relatively stable at low displacement values but decreased as displacement increased, indicating progressive structural deformation (Fig. 6b). At a displacement amplitude of 1 µm, E' ranged from 28.0 MPa to 115.1 MPa. Specifically, scaffolds printed in horizontal setup orientation presented a greater stiffness than their vertically printed counterparts ($p = 0.01$ A2 scaffolds; $p = 0.42$ A3 scaffolds; $p < 0.001$ C2 scaffolds). Among all

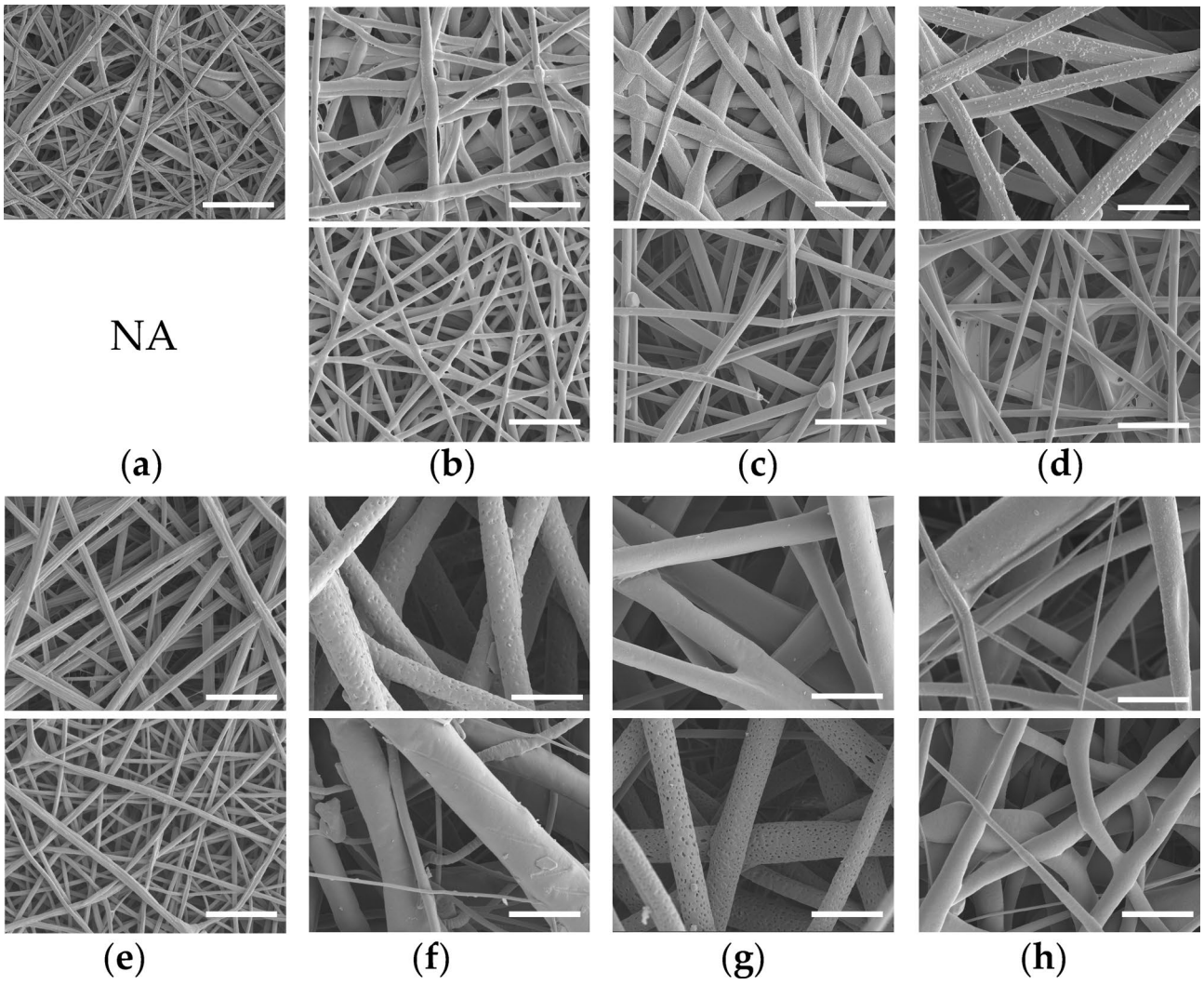


**Fig. 3**. Scanning electronic microscopy (SEM) images from (**a**) A1 scaffolds (**b**) A2 scaffolds, (**c**) A3 scaffolds, (**d**) A4 scaffolds, (**e**) A5 scaffolds, (**f**) C1 scaffolds, (**g**) C2 scaffolds, and (**h**) D1 scaffolds spun in vertical (upper panel) and horizontal (lower panel) setup orientation. Scale bar: 10 µm. NA = not available because the scaffold presented with beads. Images are representative of three independent experiments in triplicate ($n = 3$).

| | Vertical set orientation | | Horizontal set orientation | |
|---|---|---|---|---|
| Scaffold | Pore area (µm$^2$) | Fiber diameter (µm) | Pore area (µm$^2$) | Fiber diameter (µm) |
| A1 | 53.70 ± 6.04 | 0.77 ± 0.04 | – | – |
| A2 | 60.94 ± 7.01 | 1.34 ± 0.13 | 24.69 ± 2.82 | 1.05 ± 0.05 |
| A3 | 99.98 ± 3.51 | 1.77 ± 0.19 | 111.80 ± 2.55 | 1.44 ± 0.18 |
| A4 | 127.41 ± 10.59 | 2.63 ± 0.21 * | 81.75 ± 7.18 | 1.25 ± 0.12 |
| A5 | 98.66 ± 7.94 | 1.45 ± 0.09 | 36.11 ± 3.90 | 0.99 ± 0.08 |
| C1 | 467.03 ± 29.99** | 4.72 ± 0.12 | 316.08 ± 24.74 | 4.40 ± 0.48 * |
| C2 | 983.67 ± 22.13*** | 4.66 ± 0.09 | 945.18 ± 23.20 *** | 4.05 ± 0.35 |
| D1 | 462.05 ± 50.05 | 2.94 ± 0.07 | 258.09 ± 26.16 | 2.64 ± 0.21 |

**Table 2**. Pore area and fiber diameter of scaffolds after sterilization by 1 h immersion in 70% ethanol and 30 min UV exposure (each side). Data are represented as mean ± SEM of three independent experiments in triplicate ($n = 3$). Levels of statistically significance are indicated as *($p < 0.050$), **($p < 0.010$), and ***($p < 0.001$) compared with the same scaffold before sterilization.

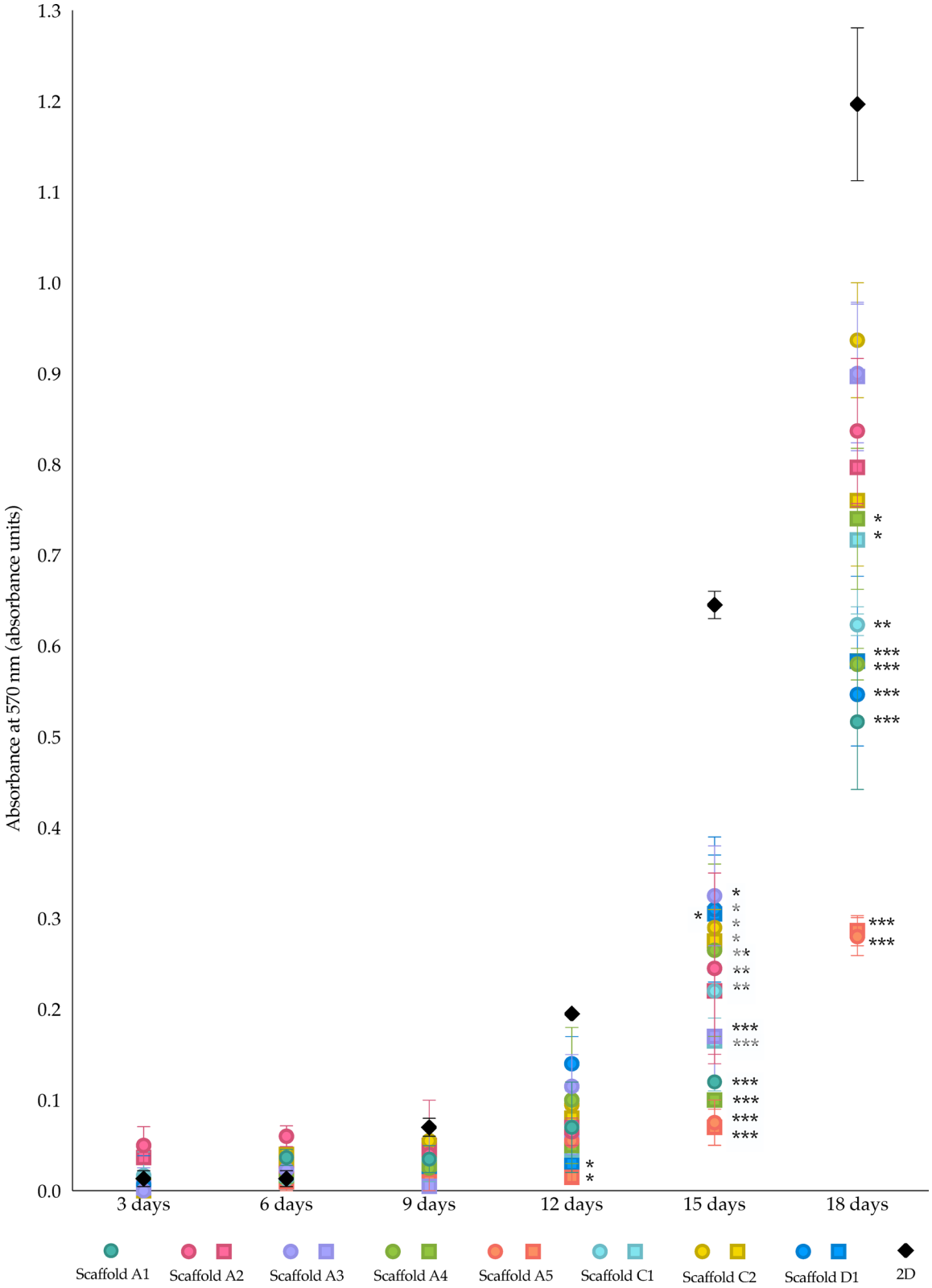


**Fig. 4**. Cell proliferation of MDA-MB-231 cells cultured in monolayer (2D) or three-dimensional scaffolds. Data are represented as mean ± SEM of all the scaffolds from three independent experiments in duplicate ($n = 3$). Levels of statistically significance are indicated as *($p < 0.050$), **($p < 0.010$), and ***($p < 0.001$) compared to 2D conditions. Setup orientation is represented by symbol shape (circle: vertical; square: horizontal).

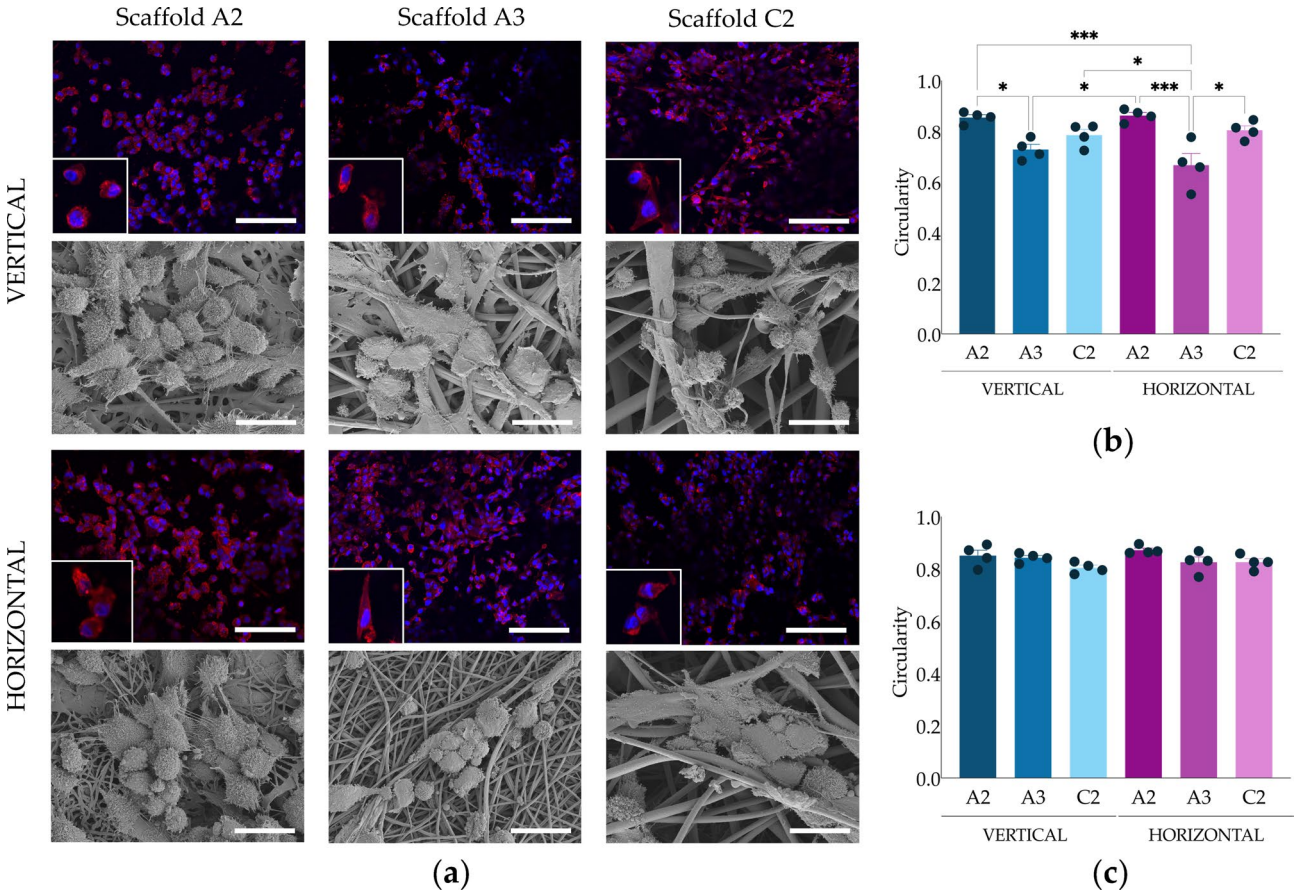


**Fig. 5**. (**a**) Confocal laser scanning microscopy (CLSM) images (upper panel) and scanning electronic microscopy (SEM) images (lower panel) from A2, A3 and C2 scaffolds spun in vertical or horizontal. Scale bar: 20 µm (SEM); 100 µm (CLSM) and enlarged picture (x3). Cells for CLSM imaging were fixed and immunostained using rhodamine-phalloidin (red) and DAPI (blue). Images are representative of four independent experiments in duplicate ($n = 4$). (**b**) Cytoplasm and (**c**) nucleus circularity of MDA-MB-231 cells cultured on A2, A3 and C2 scaffolds. Value equal to 1 means a circle and 0 no-circle. Data are represented as mean ± SEM of all the scaffolds from four independent experiments in duplicate ($n = 4$). Levels of statistically significance are indicated as *($p < 0.050$), **($p < 0.010$), and ***($p < 0.001$).

tested scaffolds, A3 scaffolds consistently exhibited the highest storage modulus across all displacement values, indicating its superior mechanical strength compared to A2 and C2 scaffolds. Furthermore, a correlation analysis between E' values and cell morphology revealed a strong negative correlation ($r$= -0.849, $p = 0.032$), indicating that higher scaffold stiffness promotes an elongated cytoplasmic morphology in cells. Overall, scaffold stiffness plays a key role in cell morphology. While polymer composition, setup orientation, and solvent selection do not directly impact cell morphology through hydrophobicity, they play a significant role in modulating scaffold stiffness, which in turn affects cellular behavior.

## Discussion

The influence of polymer composition, solvent choice, and electrospinning setup orientation on the microstructure of scaffolds has been well-documented in the literature[15,18,21,25,26]. The findings from this study provide further evidence of their interdependent impact, demonstrating how variations in these parameters influence scaffold architecture, which in turn affect cell adhesion, morphology, and proliferation. Notably, all scaffolds spun using the solvent solvent B presented with non-fibrous structures, referred to as beads. These structures produce low cell attachment and proliferation[24]reason why scaffolds containing beads were eliminated from the further experiments of the study. Beads have been related to low solvent volatility, as the higher boiling point contributes to the reduced evaporation rate during electrospinning, leading to bead formation[25,26]. This observation aligns with our results as solvent B (99.3 °C) has the highest boiling point amongst the tested solvents, compared to solvent A (60.1 °C), solvent C (53.4 °C), and solvent D (56 °C).

While comparing pore area and fiber diameter with previous studies is challenging due to the limited research on the specific combination of PS/PCL polymers[13,15,27,28] and the solvents studied[13–15,18,20,27,29,30]the data obtained in this study falls within the range of values reported in the literature. The SEM-based microstructural analysis revealed distinct differences in pore area and fiber diameter, both before and after sterilization, depending on the electrospinning setup orientation, solvent choice, and polymer composition. These differences are critical as they

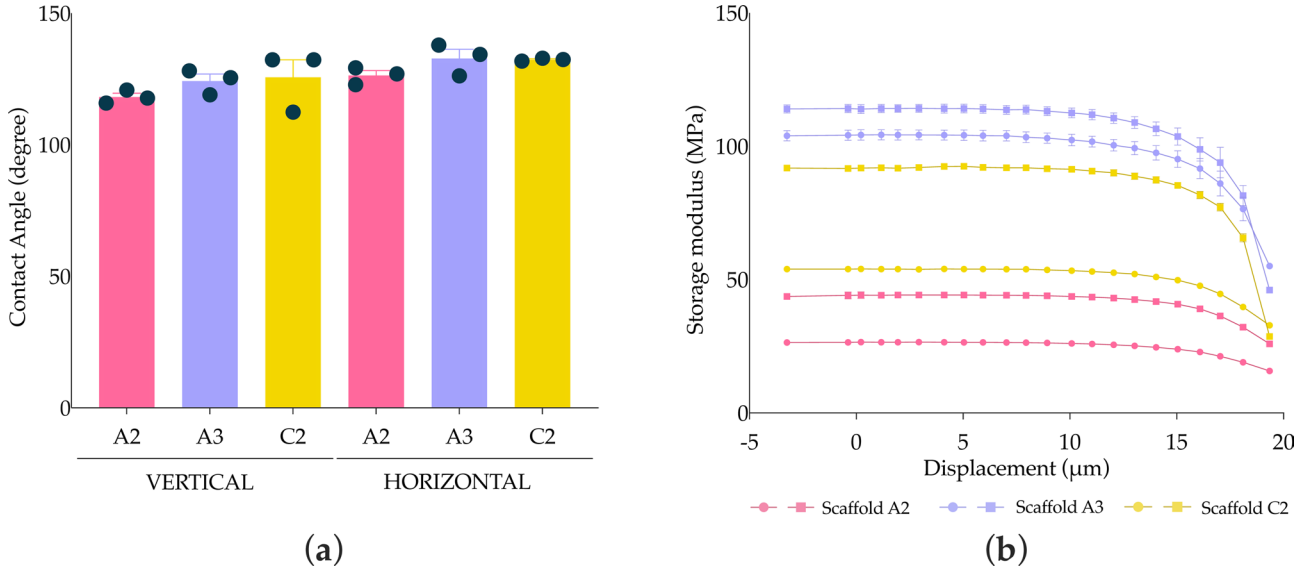


**Fig. 6**. (**a**) Water Contact Angle (WCA) measurements of A2, A3 and C2 scaffolds spun in both vertical and horizontal orientations. Data are represented as mean ± SEM of all the scaffolds from three independent experiments in duplicate ($n = 3$). (**b**) Storage modulus (E') as a function of displacement for A2, A3 and C2 scaffolds, obtained from Dynamic Mechanical Analysis (DMA). Data are represented as mean ± SEM of all the scaffolds from three independent experiments in duplicate ($n = 3$). Setup orientation is represented by symbol shape (circle: vertical; square: horizontal).

influence the ability of scaffolds to support TNBC cell growth and proliferation. Notably, the trend of increased pore area and fiber diameter in vertically spun scaffolds, compared to those spun horizontally, is consistent across various polymer compositions and solvent combinations, corroborating findings from other studies[21,31,32]. Moreover, the significant differences observed in pore area and fiber diameter between scaffolds produced with different solvent combinations further underscore the importance of solvent selection in electrospinning. Notably, scaffolds produced with solvent C and D exhibited larger pore areas and fiber diameters compared to those fabricated with solvent A and B. This may be attributed to the varying volatility of solvents, which affect fiber formation during electrospinning[13–15,18,20,27,29,30]. Additionally, the concentration of PS and PCL also impacts fiber diameter, with higher PCL concentrations and lower PS concentrations resulting in increased fiber diameter, as reported in previous studies[13].

Sterilization is a critical step when preparing scaffolds for cell culture, with high impact on scaffold structural microarchitecture[33]. This study identified the optimal sterilization method, which minimizes structural damage while ensuring complete sterilization, as a 1-hour immersion in 70% ethanol followed by 30 min of UV exposure on each side of the scaffold. This method was the shortest effective procedure that resulted in no contamination across all tested scaffolds, which aligns with previous studies that have demonstrated the efficacy of similar sterilization techniques[15,34,35]. Additionally, the observed weight increase, which indicate the degree of polymer degradation, was significantly lower with this method compared to more aggressive sterilization procedures. Although some studies have found a reduction in weight upon sterilization[33,35]others have observed similar results to us[11,18]. We attribute the weight increase to ethanol absorption by the scaffold and, since UV does not produce an immediate ethanol evaporation, the combined use of both methods result in similar weight increases. Visual changes in the scaffolds following sterilization can be attributed mostly to photodegradation resulting from UV exposure, as literature states clear photodegradation upon UV light exposure and little impact on scaffold surface morphology after immersion in 60–80% ethanol solution[34,35]. Regarding the observed trend towards thicker fibers and larger pore areas after the sterilization process, these alterations were generally not statistically significant and align with previous studies[34]. This supports the conclusion that the selected sterilization method is minimally harmful to the structural integrity of the scaffolds.

The microarchitecture of scaffolds plays a critical role in influencing 3D cell attachment and proliferation, as extensively demonstrated in the literature[9,12,36,37]. The cell viability assays conducted over an 18-day period highlighted these differences in cell proliferation across various scaffold microstructures. Although no significant differences were observed in the early stages of culture, some differences appeared as cell confluence increased. By day 18, most scaffolds demonstrated lower cell viability compared to 2D monolayer cultures. This observation aligns with previous studies[9]suggesting that the microstructure of these specific scaffolds may be less supportive of long-term TNBC cell culture. In contrast, comparable proliferation rates to 2D cultures was seen on certain scaffolds at 18-days culture, specifically A2, A3 and C2 scaffolds, regardless of setup orientation. Thus, these specific scaffolds may provide more favorable microenvironments for effective 3D TNBC cell culture, highlighting their potential as superior substrates for further investigation.

Regarding cell morphology, MDA-MB-231 breast cancer cells exhibited distinct morphological differences depending on scaffold composition, with a more rounded cytoplasm when cultured on A2 and C2 scaffolds and

an elongated cytoplasm in A3 scaffolds. These variations in cell shape can be attributed to differences in scaffold microstructure. C2 scaffolds, which exhibited thicker fibers and larger pore areas, could potentially influence cell adhesion and spreading, leading to a more rounded morphology. In contrast, A2 scaffolds presented the thinnest filaments and smaller pore areas, which could create a more confined environment restraining cell spreading, favoring a more rounded morphology. Finally, A3 scaffolds featured pore areas larger than cell size (99.98 µm2 to 11.80 µm2), yet maintained a higher fiber density, thereby increasing the surface area available for cell attachment[16,38]—which we hypothesize to be ideal for cells to spread and present elongated shapes. Literature regarding this topic presents varying perspectives, some studies report results suggesting that thicker fibers and large pore areas lead to elongated cytoplasm morphology[39,40] whereas others align with our observations[41].

Additionally, cells with elongated cytoplasm and prolongations were more prevalent in A3 scaffolds (with a polymer composition of 40% PS and 60% PCL) than in A2 and C2 scaffolds (with a polymer composition of 20% PS and 80% PCL, regardless of solvent combination). This suggests that polymer composition may play a role in guiding cellular behavior. Given that hydrophobicity is known to modulate cell adhesion, potentially promoting cell elongation as cells attempt to maximize their contact area[23,42]we initially hypothesized that changes in hydrophobicity might explain the observed differences in morphology. Hovewer, WCA measurements indicated no significant differences in hydrophobicity across scaffolds, regardless of polymer composition, solvent selection, or printing orientation. Thus, no correlation was found between hydrophobicity and cell morphology, suggesting that other physicochemical properties, such as scaffold stiffness, may be driving these differences.

Scaffold stiffness has been extensively studied as a key regulator of tumor cell behavior, influencing proliferation, invasion, and mechanotransduction signaling[43]. Given that PS is inherently stiffer than PCL[18]we hypothesized that the increased PS content in A3 scaffolds compared to A2 and C2 scaffolds, likely enhanced the scaffold stiffness, leading to increased MDA-MB-231 cell elongation. In this regard, our DMA results confirm this hypothesis, demonstrating that A3 scaffolds consistently exhibited the highest E' across all displacement values, indicating superior mechanical strength compared to A2 and C2 scaffolds. Variations in PS/PCL ratio, solvent choice, and printing orientation were shown to modulate the mechanical properties of electrospun scaffolds, ultimately affecting cell shape and behavior. These results reinforce the idea that mechanical tuning is a crucial factor in scaffold design, as stiffness can be strategically manipulated to guide cellular responses in biomaterial applications.

As stated in the literature, cell morphology modifications (such as cell elongation and irregularity) driven by ECM lead to enhanced invasion and metastatic characteristics[44,45]. Additionally, CSCs are strongly associated with metastasis and tumor invasion[4]. Therefore, despite scaffolds presented similar cell proliferation rates, A3 scaffolds (PS/PCL 40/60 (DCM/DMF) spun in both setup orientation) exhibited elongated cell morphologies, suggesting a potential enrichment of the CSCs population. This makes A3 scaffolds the most suitable candidates for further studies to validate CSCs enrichment and establish them as a robust model for investigating TNBC characteristics and progression in 3D conditions. These findings highlight the importance of solvent choice, the specific combination of PS and PCL and printing setup orientation in defining scaffold structural and mechanical properties, which subsequently affect cell behavior. Thus, the strategic selection of these parameters emerges as a promising approach to optimizing scaffold design for more accurate and predictive cancer models.

## Conclusions

To our knowledge, this is the first study that comprehensively analyzes the combined effects of setup orientation, solvent selection, and polymer composition on the development of effective 3D culture systems for TNBC research. While previous studies have examined these parameters individually, our work highlights their interdependent influence on scaffold architecture and cellular responses. Our findings underscore the pivotal role of scaffold design and processing parameters in cell behavior, highlighting the need for careful consideration of these factors in future studies aimed at creating optimized *in vitro* models for TNBC studies. Future research should build on these findings by further investigating the selected scaffolds, particularly focusing on whether protein and gene expression profiles indicate an enrichment of CSCs in 3D cell culture, to further optimize scaffold design for more accurate and predictive cancer models. The insights gained from this work offer valuable guidance for advancing scaffold-based 3D cell culture systems in cancer research, with potential applications extending to other tissue engineering areas.

## Data availability

Data is provided within the manuscript or supplementary information files.

Received: 21 January 2025; Accepted: 4 June 2025
Published online: 01 July 2025

## References

1. Cancer Today. *World Health Organization (WHO). Global Cancer Observatory (GLOBOCAN)* belbel.
2. Xiong, N., Wu, H. & Yu, Z. Advancements and challenges in triple-negative breast cancer: a comprehensive review of therapeutic and diagnostic strategies. *Front Oncol.* **14**, (2024).
3. Baranova, A. et al. Triple-negative breast cancer: current treatment strategies and factors of negative prognosis. *J. Med. Life*. **15**, 153–161 (2022).
4. Najafi, M., Farhood, B. & Mortezaee, K. Cancer stem cells (CSCs) in cancer progression and therapy. *J. Cell. Physiol.* **234**, 8381–8395 (2019).
5. Jubelin, C. et al. Three-dimensional in vitro culture models in oncology research. *Cell. Biosci.* **12**, 155 (2022).
6. Kapałczyńska, M. et al. 2D and 3D cell cultures – a comparison of different types of cancer cell cultures. *Arch. Med. Sci.* **14**, 910–919 (2018).

7. Costard, L. S., Hosn, R. R., Ramanayake, H., O'Brien, F. J. & Curtin, C. M. Influences of the 3D microenvironment on cancer cell behaviour and treatment responsiveness: A recent update on lung, breast and prostate cancer models. *Acta Biomater.* **132**, 360–378 (2021).
8. Rijal, G. & Li, W. 3D scaffolds in breast cancer research. *Biomaterials* **81**, 135–156 (2016).
9. Rabionet, M., Yeste, M., Puig, T. & Ciurana, J. Electrospinning PCL scaffolds manufacture for three-dimensional breast cancer cell culture. *Polymers* **9**, 328 (2017).
10. Florczyk, S. J. et al. 3D porous chitosan–alginate scaffolds promote proliferation and enrichment of cancer stem-like cells. *J. Mater. Chem. B*. **4**, 6326–6334 (2016).
11. Polonio-Alcalá, E. et al. Polycaprolactone electrospun scaffolds produce an enrichment of lung cancer stem cells in sensitive and resistant EGFRm lung adenocarcinoma. *Cancers (Basel)*. **13**, 5320 (2021).
12. Rahmati, M. et al. Electrospinning for tissue engineering applications. *Prog. Mater. Sci.* **117**, 100721 (2021).
13. Nguyen, T. H. & Lee, B. T. In vitro and in vivo studies of rhBMP2-coated PS/PCL fibrous scaffolds for bone regeneration. *J. Biomed. Mater. Res. A*. **101**, 797–808 (2013).
14. Jarusuwannapoom, T. et al. Effect of solvents on electro-spinnability of polystyrene solutions and morphological appearance of resulting electrospun polystyrene fibers. *Eur. Polymer J.* **41**, 409–421 (2005).
15. Pareja, M., Casanova, E., de Ciurana Gay, J., Polonio Alcalá, E. & Puig Miquel, T. Preliminary screening of polycaprolactone-polystyrene electrospun scaffolds for the formation of tumoroids. In *CASEIB 2023. Libro de Actas del XLI Congreso Anual de la Sociedad Española de Ingeniería Biomédica: Contribuyendo a la salud basada en valor*, ISBN 978-84-17853-76-1, 178–181 178–181 (Universidad Politécnica de Cartagena, 2023).
16. Echeverria Molina, M. I., Malollari, K. G. & Komvopoulos, K. Design challenges in polymeric scaffolds for tissue engineering. *Front. Bioeng. Biotechnol.* **9**, 617141 (2021).
17. Melo, G. H. F. & Sundararaj, U. Influence of mixed solvent in the morphology and hydrophobicity of electrospun polystyrene porous fibers. *Macromol. Rapid Commun.* n/a, 2400403 .
18. Polonio-Alcalá, E., Casanova-Batlle, E., Puig, T. & Ciurana, J. The solvent chosen for the manufacturing of electrospun polycaprolactone scaffolds influences cell behavior of lung cancer cells. *Sci. Rep.* **12**, 19440 (2022).
19. Ho, M. H. et al. Effects of an acetic acid and acetone mixture on the characteristics and scaffold–cell interaction of electrospun polycaprolactone membranes. *Appl. Sci.* **9**, 4350 (2019).
20. Kulpreechanan, N., Bunaprasert, T. & Rangkupan, R. Electrospinning of polycaprolactone in dichloromethane/dimethylformamide solvent system. *Adv. Mater. Res.* **849**, 337–342 (2013).
21. Suresh, S., Gryshkov, O. & Glasmacher, B. Impact of setup orientation on blend electrospinning of poly-ε-caprolactone-gelatin scaffolds for vascular tissue engineering. *Int. J. Artif. Organs*. **41**, 801–810 (2018).
22. Polonio-Alcalá, E. et al. PLA electrospun scaffolds for three-dimensional triple-negative breast cancer cell culture. *Polymers* **11**, 916 (2019).
23. Moghadas, H., Saidi, M. S., Kashaninejad, N., Kiyoumarsioskouei, A. & Nguyen, N. T. Fabrication and characterization of low-cost, bead-free, durable and hydrophobic electrospun membrane for 3D cell culture. *Biomed. Microdevices*. **19**, 74 (2017).
24. Chen, M., Patra, P. K., Lovett, M. L., Kaplan, D. L. & Bhowmick, S. Role of electrospun fibre diameter and corresponding specific surface area (SSA) on cell attachment. *J. Tissue Eng. Regen Med.* **3**, 269–279 (2009).
25. Haider, A., Haider, S. & Kang, I. K. A comprehensive review summarizing the effect of electrospinning parameters and potential applications of nanofibers in biomedical and biotechnology. *Arab. J. Chem.* **11**, 1165–1188 (2018).
26. Abdulhussain, R., Adebisi, A., Conway, B. R. & Asare-Addo, K. Electrospun nanofibers: exploring process parameters, polymer selection, and recent applications in pharmaceuticals and drug delivery. *J. Drug Deliv. Sci. Technol.* **90**, 105156 (2023).
27. Makwana, P., Modi, U., Dhimmar, B. & Vasita, R. Design and development of in-vitro co-culture device for studying cellular crosstalk in varied tissue microenvironment. *Biomaterials Adv.* **163**, 213952 (2024).
28. Lv, J. et al. Superhydrophobic PCL/PS composite nanofibrous membranes prepared through solution blow spinning with an airbrush for oil adsorption. *Polym. Eng. Sci.* **59**, E171–E181 (2019).
29. Du, L., Xu, H., Zhang, Y. & Zou, F. Electrospinning of polycaprolatone nanofibers with DMF additive: the effect of solution proprieties on jet perturbation and fiber morphologies. *Fibers Polym.* **17**, 751–759 (2016).
30. Duzyer Gebizli, S., Cunayev, S., Koral Koc, S., Tezel, S. & Peksoz, A. Influence of solvent system on the optoelectrical properties of pcl/carbon black nanofibers. *Fullerenes Nanotubes Carbon Nanostruct.* **30**, 814–819 (2022).
31. Wunner, F. M. et al. Electrospinning writing with molten Poly (ε-caprolactone) from different directions – Examining the effects of gravity. *Mater. Lett.* **216**, 114–118 (2018).
32. Suresh, S., Becker, A. & Glasmacher, B. Impact of apparatus orientation and gravity in electrospinning—A review of empirical evidence. *Polymers* **12**, 2448 (2020).
33. Rediguieri, C. F., Sassonia, R. C., Dua, K., Kikuchi, I. S. & De Jesus Andreoli pinto, T. Impact of sterilization methods on electrospun scaffolds for tissue engineering. *Eur. Polymer J.* **82**, 181–195 (2016).
34. Łopianiak, I. & Butruk-Raszeja, B. A. Evaluation of sterilization/disinfection methods of fibrous polyurethane scaffolds designed for tissue engineering applications. *Int. J. Mol. Sci.* **21**, 8092 (2020).
35. Guerra, A. J., Cano, P., Rabionet, M., Puig, T. & Ciurana, J. Effects of different sterilization processes on the properties of a novel 3D-printed polycaprolactone stent. *Polym. Adv. Techs.* **29**, 2327–2335 (2018).
36. Ghaedamini, S., Hashemibeni, B., Honarvar, A., Rabiei, A. & Karbasi, S. Recent innovations in strategies for breast cancer therapy by electrospun scaffolds: A review. *J. Polym. Environ.* **32**, 1001–1027 (2024).
37. Hodge, J. & Quint, C. The improvement of cell infiltration in an electrospun scaffold with multiple synthetic biodegradable polymers using sacrificial PEO microparticles. *J. Biomed. Mater. Res. A*. **107**, 1954–1964 (2019).
38. Amores de Sousa, M. C. et al. Functionalization of electrospun nanofibers and fiber alignment enhance neural stem cell proliferation and neuronal differentiation. *Front. Bioeng. Biotechnol.* **8**, 580135 (2020).
39. English, A. et al. Substrate topography: A valuable *in vitro* tool, but a clinical red herring for *in vivo* tenogenesis. *Acta Biomater.* **27**, 3–12 (2015).
40. Jenkins, T. L. & Little, D. Synthetic scaffolds for musculoskeletal tissue engineering: cellular responses to fiber parameters. *NPJ Regen Med.* **4**, 15 (2019).
41. Tylek, T. et al. Precisely defined fiber scaffolds with 40 μm porosity induce elongation driven M2-like polarization of human macrophages. *Biofabrication* **12**, 025007 (2020).
42. Slivac, I. et al. Bioactivity comparison of electrospun PCL Mats and liver extracellular matrix as scaffolds for HepG2 cells. *Polymers* **13**, 279 (2021).
43. Yui, A. & Oudin, M. J. The rigidity connection: matrix stiffness and its impact on cancer progression. *Cancer Res.* **84**, 958–960 (2024).
44. Conner, S. J. et al. Cell morphology best predicts tumorigenicity and metastasis in vivo across multiple TNBC cell lines of different metastatic potential. *Breast Cancer Res.* **26**, 43 (2024).
45. Baskaran, J. P. et al. Cell shape, and not 2D migration, predicts extracellular matrix-driven 3D cell invasion in breast cancer. *APL Bioeng.* **4**, 026105 (2020).

## Acknowledgements
The authors acknowledge the Sira Ausellé-Bosch pre-doctoral Grants (2024 FI-1 00866 and FPU23/03896), the support of Catalan Government (2021SGR01589) and Oncolliga Foundation and RadikalSwim (OncoSwim). The authors express their gratitude to Dr. Joaquim Ciurana for the provision of laboratory facilities and to Mr. Enric Casanova-Batlle for the development of the software utilized for the analysis of the scaffold microarchitecture.

## Author contributions
Conceptualization, S.A. and E.P.; Data curation, S.A.; Formal analysis, S.A.; Funding acquisition, T.P.; Investigation, S.A., M.P.M., and M.P.J.; Methodology, S.A.; Project administration, S.A., M.P.M., and T.P.; Resources, T.P.; Supervision, T.P.; Validation, S.A.; Visualization, S.A. and M.P.M.; Writing – original draft, S.A.; Writing – review & editing, M.P.M., M.P.J., E.P., and T.P.

## Funding
This research was funded by Fundación Ramón Areces, Instituto de Salud Carlos III and co-funded by European Union (ERDF/ESF, "A way to make Europe"/"Investing in your future") (PI19/00372). It was also supported by PLEC2021-007523/AEI/10.13039/501100011033 and by the European Union NextGenerationEU.

## Declarations

## Competing interests
The authors declare no competing interests.

## Additional information
**Supplementary Information** The online version contains supplementary material available at https://doi.org/10.1038/s41598-025-05871-8.

**Correspondence** and requests for materials should be addressed to T.P.

**Reprints and permissions information** is available at www.nature.com/reprints.

**Publisher's note** Springer Nature remains neutral with regard to jurisdictional claims in published maps and institutional affiliations.